# Superradiance from Two Dimensional Brick-Wall Aggregates of Dye Molecules: The Role of Size and Shape for the Temperature Dependence

Alexander Eisfeld,[1,*] Christian Marquardt,[2] Alexander Paulheim,[2] and Moritz Sokolowski[2]
[1]*Max-Planck-Institut für Physik komplexer Systeme, Nöthnitzer Str. 38, D-01187 Dresden, Germany*
[2]*Universität Bonn, Institut für Physikalische und Theoretische Chemie, Wegelerstr. 12, 53115 Bonn, Germany*
(Received 10 November 2016; revised manuscript received 10 June 2017; published 31 August 2017)

Aggregates of interacting molecules can exhibit electronically excited states that are coherently delocalized over many molecules. This can lead to a strong enhancement of the fluorescence decay rate which is referred to as superradiance (SR). To date, the temperature dependence of SR is described by a $1/T$ law. Using an epitaxial dye layer and a Frenkel-exciton based model we provide both experimental and theoretical evidence that significant deviations from the $1/T$ behavior can occur for brick-wall-type aggregates of finite size leading even to a maximum of the SR at finite temperature. This is due to the presence of low energy excitations of weak or zero transition strength. These findings are relevant for designing light-emitting molecular materials.

DOI: 10.1103/PhysRevLett.119.097402

Aggregates of fluorescent dye molecules are of great interest not only for various technological applications, e.g., organic light-emitting displays, but also as model systems for studying the delocalization of electronic excitations in many-particle physics. Often in these aggregates the distances between the molecules are so large that there is negligible overlap of electronic wave functions; i.e., there is no exchange of electrons. However, the molecules can exchange electronic excitation via transition dipole-dipole interaction. This can have a strong effect on their optical properties [1–3]. Some aggregates show an enhancement in the fluorescence emission rate of a single electronic excitation compared to that of the individual, noninteracting monomers. This phenomenon is generally referred to as superradiance (SR). (It is related to the general concept of SR introduced by Dicke [4], but in the present case restricted to a single optical excitation [5].) Superradiant molecular aggregates have been extensively investigated experimentally [6–16] and theoretically [17–24].

The SR depends strongly on temperature. In several studies a $1/T$ decay of the SR was observed (see, e.g., Refs. [11,12]). It is explained by an excited lowest energy state of high transition strength (TS) that dominates at low temperature, but is thermally depopulated at the expense of states at higher energies with reduced TS. This "canonical" situation is generally encountered for typical 1D $J$ aggregates of infinite and finite size with parallel arrangement of the transition dipoles [1].

Here we provide experimental and theoretical results demonstrating that strong deviations from this $1/T$ behavior are possible for 2D aggregates with a brick-wall-type arrangement of the transition dipoles and a finite size of $N_x \times N_y$ molecules (cf. inset in Fig. 1). The temperature dependence of the SR yields direct information on the excited states and their energetic spectrum and indirect information on the intermolecular coupling. The 2D brick-wall arrangement bears competing negative interactions (mainly along the direction of the transition dipoles) and positive interactions (mainly in the direction perpendicular to the transition dipoles). As we will demonstrate, this can result in antisymmetric (with respect to the center of the aggregate) excitonic multiparticle wave functions of the lowest excited eigenstate. These wave functions lead to destructive interference of the molecular transition dipoles, causing vanishing TS. As a consequence, for certain aggregate sizes and shapes, at small temperatures an *increase* of the fluorescence with increasing temperature is possible, contrary to the established $1/T$ behavior.

Our experiments were performed on 2D aggregates prepared by epitaxial growth of about one layer of the perylene-type dye PTCDA (see Fig. 1) on the (100) surface of KCl [25,26]. This surface promotes the arrangement of the PTCDA molecules in ordered aggregates of the brick-wall type as illustrated in Fig. 1(a). The transition dipole $\vec{\mu}$ of the PTCDA molecules is parallel to the long molecular axis. The details and the optical spectra of this structure were described in Ref. [27]. One important aspect of our experimental system is that effects such as static disorder or strong exciton-phonon coupling that typically complicate the interpretation of observations are very small, as reviewed in Sec. I of the Supplemental Material [28].

For measuring the SR, the sample was excited by a weak laser beam (476 nm) and fluorescence spectra were recorded systematically under variation of the sample temperature. The SR enhancement $\eta_{\mathrm{SR}}$ is defined via the change in the radiative decay rate, namely, $k_{\mathrm{rad}}^{\mathrm{aggregate}}/k_{\mathrm{rad}}^{\mathrm{monomer}}$. For its experimental determination we use the procedure described by Spano, which exploits the increase of the intensity of the pure electronic transition without excitation of an additional vibron ($I_{0-0}$) relative to

 

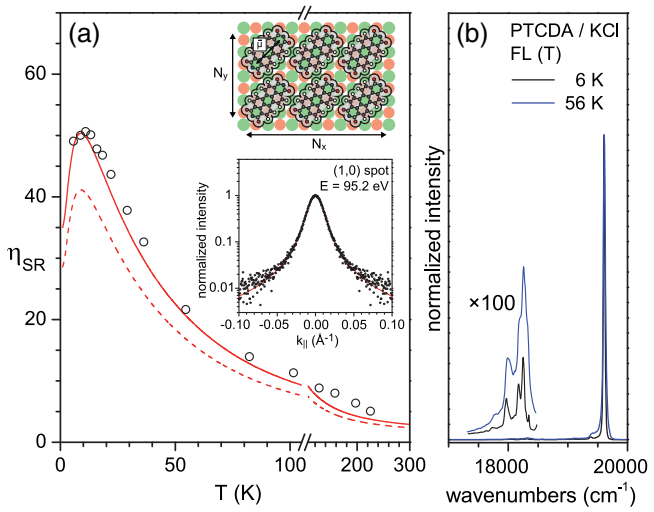


FIG. 1. (a) Enhancement factor $\eta_{\mathrm{SR}}$ of the superradiance as a function of temperature. The open circles show experimental data for a monolayer of PTCDA on the KCl (100) surface. Note the maximum of $\eta_{\mathrm{SR}}^{\mathrm{max}} = 50$ at $T \approx 16$ K. The dashed line is calculated for a geometric distribution of aggregates sizes with an average size of $\langle N_x \times N_y \rangle = 12.4 \times 12.4$ molecules (cf. Fig. 3) determined from the LEED Profile. The solid line was multiplied by an additional factor of 1.2 adapting the theoretical curve to the experimental situation (for details see the Supplemental Material [28]). Inset top: Hard sphere model of a $3 \times 2$ aggregate of PTCDA molecules on the KCl (100) surface. The transition dipole moment $\vec{\mu}$ is depicted for the top left molecule. Inset bottom: Experimental and fitted LEED profile of the PTCDA (1,0) spot using the above mentioned geometric aggregate size distribution. More details are given in the SI. (b) Fluorescence (FL) spectra normalized at the 0-0 transition (19600 $\mathrm{cm}^{-1}$) at 6 and 56 K illustrating the enhancement of the 0-0 transition with respect to the vibronic peaks due to superradiance.

the intensity of transitions to vibrational excited states ($I_{0-1}$) [24] [cf. Fig. 1(b)]. Our procedure is described in Ref. [27] and additional details on its validity are provided in the Supplemental Material [28]. The obtained SR enhancement $\eta_{\mathrm{SR}}$ versus temperature curve is displayed in Fig. 1(a).

In our experiments, the surface is covered by aggregates separated by structural antiphase boundaries or KCl steps. As a result aggregates with a broad distribution in sizes and shapes are obtained. We determined the aggregate size distribution by a low energy electron diffraction (LEED) profile analysis. We consider aggregates of rectangular shape, with a size of $N_x \times N_y$ molecules with edges as sketched in Fig. 1.

An experimental and a fitted LEED profile are shown in the inset of Fig. 1(a). The details of the analysis are described in the Supplemental Material [28]. We find for the size distribution of the aggregates: $P_{N_x,N_y} \sim \exp(-N_x \Lambda_x^{-1}) \times \exp(-N_y \Lambda_y^{-1})$, $\Lambda_{x,y} = \ln[\Gamma_{x,y}/(\Gamma_{x,y} - 1)]$, with $\Gamma_{x,y}$ denoting the expected values of the underlying one dimensional distributions. Our analysis yields $\langle N_x \times N_y \rangle = 12.4 \times 12.4$ molecules ($\hat{=}156 \times 156$ Å$^2$). Important, because $N_x$ and $N_y$ are independent, the distribution yields also aggregates of elongated shape with aspect ratios $N_x/N_y \neq 1$. We note that due to an optimized sample preparation the average linear aggregate size was about twice as large as that reported in earlier experiments [27] (see also Supplemental Material [28]). This leads to a larger number of coherently coupled molecules. In combination with an extension of the experimental accessible temperature range to low temperatures we obtain an $\eta_{\mathrm{SR}}(T)$ dependence with new interesting features: At high temperatures ($\gtrsim 20$ K) $\eta_{\mathrm{SR}}(T)$ is roughly compatible with the noted $1/T$ dependence. However, at low $T$ $\eta_{\mathrm{SR}}$ does not decrease, but slightly increases with $T$ and goes through a maximum at a finite temperature $T_{\mathrm{max}} \approx 10$ K. This interesting behavior deserves attention.

To understand these observations we perform numerical simulations based on the Frenkel exciton model [43]. We treat each monomer as a two level system with an electronic ground state $|g\rangle$ and one electronically excited state $|e\rangle$, with energies $E_g$ and $E_e$, respectively. These two states are coupled by a transition dipole $\vec{\mu}$. The electronic ground state is taken as the state where all monomers are in their ground state, i.e., $|g_{\mathrm{agg}}\rangle = |g\rangle \cdots |g\rangle$. Fluorescence originates from states which possess a single excitation. To describe such states of the dipole-dipole interacting monomers we consider a basis of localized excitations $|n\rangle = |g\rangle \cdots |e\rangle \cdots |g\rangle$; i.e., states where one monomer $n$ is excited and all the others are in the ground state. The Hamiltonian (of one domain) is given by

$$H_{\mathrm{ex}} = \sum_n \epsilon |n\rangle\langle n| + \sum_{n,m} V_{nm} |n\rangle\langle m|. \qquad (1)$$

Here, $\epsilon = E_e - E_g$ is the energy difference between the electronic excited state and the electronic ground state, and $V_{nm}$ is the interaction strength between states $|n\rangle$ and $|m\rangle$, which we take as the point transition dipole-dipole interaction $V_{nm} = (1/4\pi\epsilon_0)(\alpha/R_{nm}^3)[\vec{\mu}_n \cdot \vec{\mu}_m - 3(\vec{\mu}_n \cdot \vec{R}_{nm})(\vec{\mu}_m \cdot \vec{R}_{nm})]$, with $\vec{R}_{nm}$ the direction between monomer $n$ and $m$ and $R_{nm}$ the corresponding distance. The scaling factor $\alpha$ is used to take into account various effects including, in particular, the Franck-Condon factor that is relevant for the interaction, cf. Ref. [27], and the polarization screening by the KCl surface. For $\alpha = 1$ the dominant interactions are presented in Fig. 1 of Ref. [27]. All interactions between nearest neighbors are negative. But there are positive interactions between next nearest neighbors perpendicular to the dipole direction. We note that in general one has to use a more sophisticated method to calculate the interactions and one also has to take internal and external vibrational modes of the molecules into account explicitly [41]. However, for the present purpose, where we aim at a qualitative understanding, we found it sufficient to use the simple form of the above given point dipole-dipole interaction.

Formally the eigenenergies and eigenstates can be written as $H_{\mathrm{ex}}|\psi_k\rangle = E_k|\psi_k\rangle$ with $|\psi_k\rangle = \sum_n c_{nk}|n\rangle$. The radiative lifetime of these states is inversely proportional to their TS [44], which are calculated as $F_k = |\langle g_{\mathrm{agg}}|\sum_n \hat{\vec{\mu}}_n|\psi_k\rangle|^2$, where $\hat{\vec{\mu}}_n$ is the dipole operator of monomer $n$. For aligned molecules with identical transition dipoles ($\vec{\mu}_n = \vec{\mu}$), as in our case, this yields $F_k = \mu^2 A_k$ with

$$A_k = \left|\sum_n c_{nk}\right|^2. \tag{2}$$

To treat finite temperatures we assume that thermalization in the excited state manifold happens fast on the time scale of radiative decay, so that one has always a Boltzmann distribution, where each excited state is populated according to $p_k(T) = (1/Z)\exp(-E_k/k_BT)$ with $Z = \sum_k \exp(-E_k/k_BT)$ and $k_B$ being the Boltzmann factor. Then the (temperature-dependent) decay rate from the excited state to the ground state is given by $F(T) = \sum_k p_k(T)F_k \equiv \mu^2\eta_{\mathrm{SR}}(T)$ [44] with the enhancement factor

$$\eta_{\mathrm{SR}}(T) = \sum_k p_k(T)A_k. \tag{3}$$

For our calculations we consider the same type of rectangular aggregates as for the LEED profile analysis. We neglect any interaggregate coupling (from our experiments we have no indication of exciton diffusion between aggregates). As in Ref. [27] we take $|\vec{\mu}| = 7.4$ D. For the calculations we use $\alpha = 0.4$. This is about twice as large as the interaction strength that is obtained when we take only the Franck-Condon factor of the 0-0 transition into account [27] and treats several of the above noted effects in an effective manner. This value of $\alpha$ is motivated because it fits the calculations to the experiment. We note that our principle findings are robust with respect to the value of $\alpha$. In Sec. II. b of the Supplemental Material [28] we treat the coupling to phonons and discuss our approximations. We note that the used value of $\alpha$ can also fit the $\eta_{\mathrm{SR}}(T)$ curve of Ref. [27].

Figure 2 presents exemplary curves from the calculations, illustrating three cases (A–C) representing different behaviors of $\eta_{\mathrm{SR}}(T)$, which are found for different aspect ratios $N_x/N_y$ of the aggregates. From top to bottom $N_y$ is increased, while $N_x = 10$ is fixed. In case A ($10 \times 10$), we find a monotonic decay of $\eta_{\mathrm{SR}}(T)$ with increasing temperature. The curve shows a fast initial decay before it decays more slowly (roughly like $1/T$). For case B ($10 \times 20$), the initial decay is very steep and followed by a slight increase leading to a local maximum and a slow decay again. Finally, in case C ($10 \times 30$), an initial increase is found followed by a decrease after a maximum. These three cases are a consequence of the different energies and corresponding TS of the lowest excited eigenstates of the different aggregates. These are illustrated together with the wave functions of the lowest states ($k = 1$) in the right column of Fig. 2.

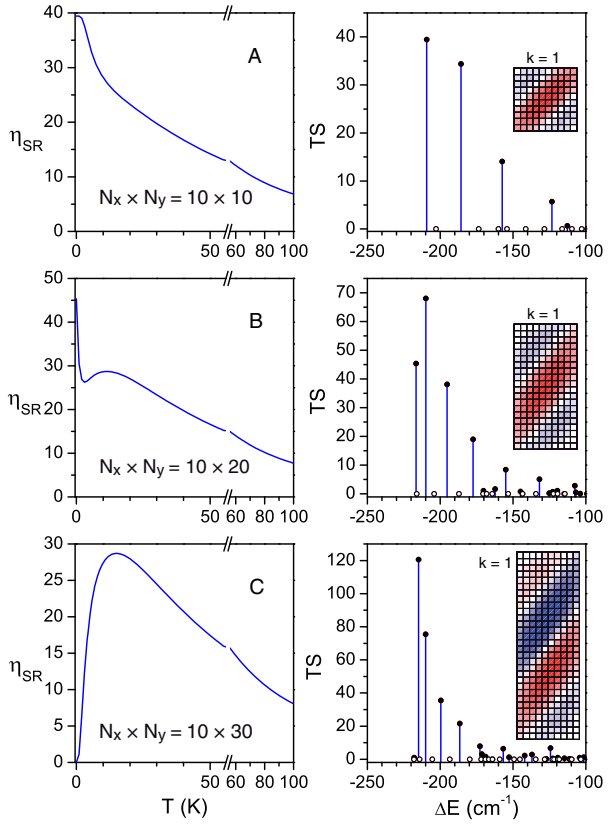


FIG. 2. Left: Temperature dependence of the enhancement factor $\eta_{\mathrm{SR}}$, according to Eq. (3) for different aggregates of $N_x \times N_y$ molecules. Right: Stick spectra of the transition strengths of the lowest eigenstates corresponding to the respective aggregates. The energies are referenced versus the excitation energy $\epsilon$ of the single molecule. The eigenstates are marked by filled (TS $> 0$) or open circles (TS $= 0$). The inset illustrates the normalized wave function of the lowest state ($k = 1$). The values of the real coefficients $c_{nk}$ are plotted with red and blue color indicating positive and negative values, respectively. Note that the two wave functions at the top are symmetric, while the lower is antisymmetric leading to TS $= 0$ for the $k = 1$ state.

To understand the $\eta_{\mathrm{SR}}(T)$ behavior we consider the energies $E_k$ and the corresponding TS ($\mu^2 A_k$) of the lowest eigenstates. Numerically, we find that if the state with the lowest energy is bright ($A_1 > 0$), then the state with the next higher energy is dark ($A_2 = 0$), and vice versa. Thus it is instructive to discuss the origin of bright and dark states as the lowest energy states. It can be understood from the wave functions illustrated in the right panel of Fig. 2 and it is an effect from the brick-wall arrangement. Important to note are the parallel node lines of the wave functions running along the direction of the transition dipoles which are a consequence of the intermolecular interactions. Because a pair of molecules $(n, m)$ contributes to the eigenenergy by $V_{nm}c_{nk}c_{mk}$ the presence of node lines turns positive interactions $V_{nm}$ between molecules separated by a

node line into negative contributions by the factor $c_{nk}c_{mk} < 0$. The interplay between negative interactions along the dipole direction (supporting $c_{nk}c_{mk} > 1$) and positive interactions in the perpendicular direction thus leads to the node lines in the wave functions. The number of node lines increases with the elongation of the aggregate. In addition the symmetry of the wave function of the lowest eigenstate can change. This is seen in Fig. 2. While the wave function is symmetric for the quadratic ($10 \times 10$) and the slightly elongated aggregate ($10 \times 20$) (2 node lines), an antisymmetric wave function (3 node lines) is formed for the strongly elongated aggregate ($10 \times 30$). Similar patterns of the wave functions with alternating symmetries are observed for larger aggregates with increasing elongation. Importantly, antisymmetric wave functions lead to zero values of TS, because the positive and negative $c_{nk}$ values cancel each other in Eq. (2). Thus the size- and shape-dependent formation of symmetric and antisymmetric wave functions of the lowest energy state leads to the occurrence of bright or dark eigenstates at the lowest energies.

In case C one will have a rise in $\eta_{\mathrm{SR}}(T)$ for increasing temperature, since bright states are thermally occupied. In the opposite case when the lowest state is bright (and the second excited state dark) one has an initial decrease of $\eta_{\mathrm{SR}}(T)$ (cases A and B). The details depend on the TS and the energy differences between the lowest states. Numerically, we found that most of the TS is located on the first 5–10 states where the ratio between bright and dark states is roughly equal. As long as the temperature is smaller than the energy difference of these states, details of the TS play a role. When the temperature becomes larger, details of the energy differences and TS of the few lowest energy states are no longer important and for all aggregate sizes one obtains a similar curve, which goes roughly like $1/T$ as expected for a single bright state at $k = 1$ and a linear density of states [24].

In Fig. 3 we present an overview of $\eta_{\mathrm{SR}}^{\mathrm{max}}$ and the corresponding temperatures $T_{\mathrm{max}}$ for which this maximum occurs for a large number of $N_x \times N_y$ combinations. In the top panel $\eta_{\mathrm{SR}}^{\mathrm{max}}$ values are displayed for different $N_x \times N_y$ aggregates. In the bottom panel the corresponding $T_{\mathrm{max}}$ values are shown, whereby regions corresponding to the three cases A, B, and C are indicated. Aggregates where $\eta_{\mathrm{SR}}^{\mathrm{max}}$ occurs at $T = 0$ (black region) are foremost found for an aspect ratio $N_x/N_y$ close to one (cases A and B), but also for $N_x$ or $N_y \leq 3$ (case A). In the latter case, node planes perpendicular to the direction of the transition dipoles cannot form due to the reduced coupling in that direction. From the top panel one sees that for symmetric aggregates $\eta_{\mathrm{SR}}^{\mathrm{max}} \sim 2(N_x + N_y)$, which is much smaller than the number of coherently coupled molecules ($N_x \times N_y$). Outside the black area, the maximum occurs at finite temperatures (case C). In the corresponding regions in the top panel one finds a clear decrease in $\eta_{\mathrm{SR}}^{\mathrm{max}}$ compared to similar aggregates located in the black region of the bottom panel. One also sees that in this region the smaller value of $N_x$ and $N_y$ determines $\eta_{\mathrm{SR}}^{\mathrm{max}}$ and the temperature $T_{\mathrm{max}}$ at which it appears.

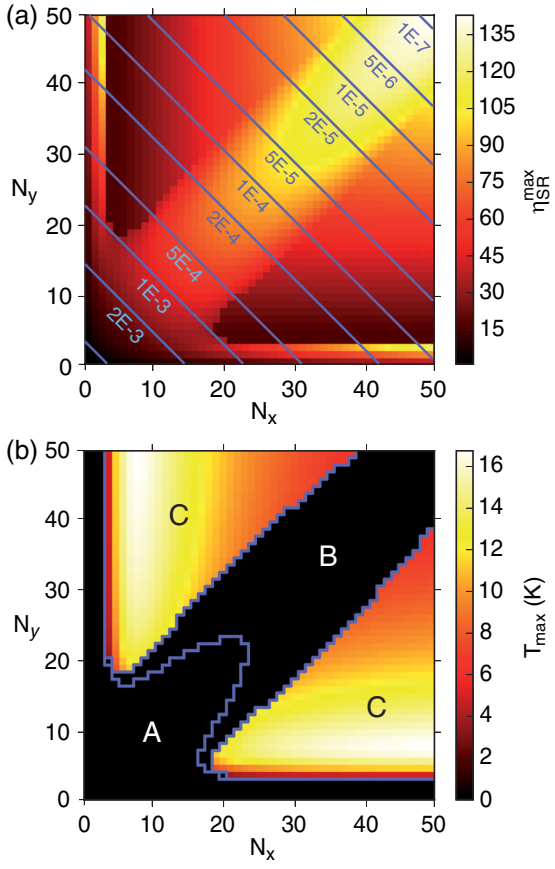


FIG. 3. (a) The maximum of the enhancement factor $\eta_{\mathrm{SR}}^{\mathrm{max}}$ for aggregates of different size $N_x \times N_y$. The blue overlayed isolines refer to the geometric aggregate size distribution used for the calculated $\eta_{\mathrm{SR}}(T)$ curve presented in Fig. 1(a). (b) The corresponding temperature $T_{\mathrm{max}}$. The regions where the three cases A, B, and C apply are indicated and separated by blue lines. For further details see text.

We finally compare to our experimental results. In Fig. 1(a), in addition to the experimental data, the calculated $\eta_{\mathrm{SR}}(T)$ curves are shown: $\eta_{\mathrm{SR}} = \sum \tilde{P}_{N_x,N_y} \cdot \eta_{\mathrm{SR}}(N_x, N_y, T)$, whereby $\tilde{P}_{N_x,N_y} = P_{N_x,N_y}(N_x \times N_y) / \sum P_{N_x,N_y}(N_x \times N_y)$. Here, results from Eq. (3) for different $N_x \times N_y$ aggregates are averaged using the probability distribution $P_{N_x,N_y}$ extracted from LEED and a geometric factor $N_x \times N_y$ accounting for the absorption cross section of the respective aggregates. The distribution $P_{N_x,N_y}$ is indicated in Fig. 3(a). We obtain a very good agreement to the shape of the experimental $\eta_{\mathrm{SR}}(T)$ curve. We note that the $\eta_{\mathrm{SR}}(T)$ curve cannot be explained by quadratic aggregates only, because then the $T$ dependence (in particular the shape) cannot be fitted. This implies that in the experiment a large number of rectangular aggregates with a ratio $N_x/N_y \neq 1$ exists, which is plausible from the two independent growth directions $x$ and

$y$, and also supported from LEED analysis (see Supplemental Material [28]).

Our theoretical and experimental results show that for 2D brick-wall aggregates the smallest temperature does not necessarily give the largest fluorescence rate. Theoretically, we have found that the temperature dependence of the enhancement can show various different behaviors, which strongly depend on the shape of aggregates. The reason is that elongated aggregates favour antisymmetric wave functions which exhibit small transition strength. Our results can be used for the design of light emitting materials, since they demonstrate that the radiative lifetime can be dramatically effected not only by the size but also by the shape of finite size molecular aggregates.

We acknowledge helpful discussions with J. Wollschläger and support by the Deutsche Forschungsgemeinschaft through the Project No. So407/8-1.

*eisfeld@mpipks-dresden.mpg.de

[1] *J-Aggregates*, edited by T. Kobayashi (World Scientific, Singapore, 1996).
[2] F. Würthner, T. E. Kaiser, and C. R. Saha-Möller, Angew. Chem., Int. Ed. Engl. **50**, 3376 (2011).
[3] S. K. Saikin, A. Eisfeld, S. Valleau, and A. Aspuru-Guzik, Nanophotonics **2**, 21 (2013).
[4] R. H. Dicke, Phys. Rev. **93**, 99 (1954).
[5] M. Gross and S. Haroche, Phys. Rep. **93**, 301 (1982).
[6] F. Meinardi, M. Cerminara, A. Sassella, R. Bonifacio, and R. Tubino, Phys. Rev. Lett. **91**, 247401 (2003).
[7] H. Z. Wang, X. G. Zheng, F. L. Zhao, Z. L. Gao, and Z. X. Yu, Phys. Rev. Lett. **74**, 4079 (1995).
[8] S.-H. Lim, T. G. Bjorklund, F. C. Spano, and C. J. Bardeen, Phys. Rev. Lett. **92**, 107402 (2004).
[9] H. Fidder, J. Knoester, and D. A. Wiersma, Chem. Phys. Lett. **171**, 529 (1990).
[10] H. Fidder, J. Terpstra, and D. A. Wiersma, J. Chem. Phys. **94**, 6895 (1991).
[11] D. H. Arias, K. W. Stone, S. M. Vlaming, B. J. Walker, M. G. Bawendi, R. J. Silbey, V. Bulović, and K. A. Nelson, J. Phys. Chem. B **117**, 4553 (2013).
[12] S. De Boer and D. A. Wiersma, Chem. Phys. Lett. **165**, 45 (1990).
[13] S. Özjcelik and D. L. Akins, J. Phys. Chem. B **103**, 8926 (1999).
[14] D. L. Akins, S. Özçelik, H.-R. Zhu, and C. Guo, J. Phys. Chem. **100**, 14390 (1996).
[15] V. F. Kamalov, I. A. Struganova, and K. Yoshihara, J. Phys. Chem. **100**, 8640 (1996).
[16] M. Müller, S. Izadnia, S. M. Vlaming, A. Eisfeld, A. LaForge, and F. Stienkemeier, Phys. Rev. B **92**, 121408 (2015).
[17] M. Orrit, C. Aslangul, and P. Kottis, Phys. Rev. B **25**, 7263 (1982).
[18] J. Grad, G. Hernandez, and S. Mukamel, Phys. Rev. A **37**, 3835 (1988).
[19] E. O. Potma and D. A. Wiersma, J. Chem. Phys. **108**, 4894 (1998).
[20] F. C. Spano and S. Mukamel, J. Chem. Phys. **91**, 683 (1989).
[21] D. J. Heijs, V. A. Malyshev, and J. Knoester, Phys. Rev. Lett. **95**, 177402 (2005).
[22] F. C. Spano, J. R. Kuklinski, and S. Mukamel, Phys. Rev. Lett. **65**, 211 (1990).
[23] F. C. Spano, Chem. Phys. Lett. **331**, 7 (2000).
[24] F. C. Spano and H. Yamagata, J. Phys. Chem. B **115**, 5133 (2011).
[25] T. Dienel, C. Loppacher, S. Mannsfeld, R. Forker, and T. Fritz, Adv. Mater. **20**, 959 (2008).
[26] M. Müller, J. Ikonomov, and M. Sokolowski, Surf. Sci. **605**, 1090 (2011).
[27] M. Müller, A. Paulheim, A. Eisfeld, and M. Sokolowski, J. Chem. Phys. **139**, 044302 (2013).
[28] See Supplemental Material at http://link.aps.org/supplemental/10.1103/PhysRevLett.119.097402 for detailed properties of the sample, details on the theoretical modeling, aspects of the determination of the superradiant enhancement from the fluorescence spectra, and the LEED profile analysis. The Supplemental Material includes Refs. [29–42].
[29] M. Müller, A. Paulheim, C. Marquardt, and M. Sokolowski, J. Chem. Phys. **138**, 064703 (2013).
[30] A. Paulheim, M. Müller, C. Marquardt, and M. Sokolowski, Phys. Chem. Chem. Phys. **15**, 4906 (2013).
[31] Q. Guo, A. Paulheim, M. Sokolowski, H. Aldahhak, E. Rauls, and W. G. Schmidt, J. Phys. Chem. C **118**, 29911 (2014).
[32] A. Paulheim, C. Marquardt, M. Sokolowski, M. Hochheim, T. Bredow, H. Aldahhak, E. Rauls, and W. G. Schmidt, Phys. Chem. Chem. Phys. **18**, 32891 (2016).
[33] A. Paulheim, C. Marquardt, H. Aldahhak, E. Rauls, W. G. Schmidt, and M. Sokolowski, J. Phys. Chem. C **120**, 11926 (2016).
[34] H. Fidder, J. Knoester, and D. A. Wiersma, J. Chem. Phys. **95**, 7880 (1991).
[35] A. Eisfeld and J. S. Briggs, Chem. Phys. **324**, 376 (2006).
[36] M. Voigt, A. Langner, P. Schouwink, J. M. Lupton, R. F. Mahrt, and M. Sokolowski, J. Chem. Phys. **127**, 114705 (2007).
[37] C. Marquardt, A. Paulheim, and M. Sokolowski, Surf. Sci. **641**, 128 (2015).
[38] J. Libuda, F. Winkelmann, M. Bäumer, H.-J. Freund, Th. Bertrams, H. Neddermeyer, and K. Müller, Surf. Sci. **318**, 61 (1994).
[39] C. S. Lent and P. I. Cohen, Surf. Sci. **139**, 121 (1984).
[40] C. Marquardt, A. Paulheim, N. Rohbohm, R. Merkel, and M. Sokolowski, Rev. Sci. Instrum. **88**, 083702 (2017).
[41] J. Roden, A. Eisfeld, M. Dvořák, O. Bünermann, and F. Stienkemeier, J. Chem. Phys. **134**, 054907 (2011).
[42] M. Henzler, Appl. Phys. A **34**, 205 (1984).
[43] J. Frenkel, Z. Phys. A **59**, 198 (1930).
[44] V. May and O. Kühn, *Charge and Energy Transfer Dynamics in Molecular Systems*, 3rd ed. (Wiley-VCH, Weinheim, 2011).